

Solution-Phase Epitaxial Growth of Quasi-Monocrystalline Cuprous Oxide on Metal Nanowires

Beniamino Sciacca,[†] Sander A. Mann,[†] Frans D. Tichelaar,[‡] Henny W. Zandbergen,[‡] Marijn A. van Huis,^{‡,§} and Erik C. Garnett*,[†]

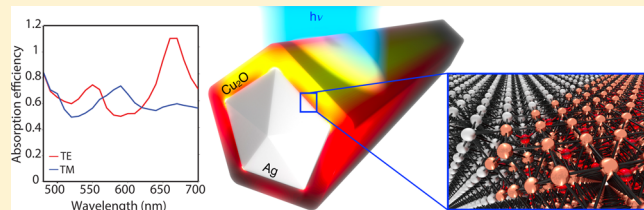
[†]Center for Nanophotonics, FOM Institute AMOLF, Science Park Amsterdam 104, 1098 XG Amsterdam, The Netherlands

[‡]National Center for HREM, Kavli Institute of Nanoscience, Delft University of Technology, Lorentzweg 1, 2628CJ, Delft, The Netherlands

[§]Debye Institute for Nanomaterials Science and Center for Extreme Matter and Emergent Phenomena, Utrecht University, Princetonplein 5, 3584CC Utrecht, The Netherlands

Supporting Information

ABSTRACT: The epitaxial growth of monocrystalline semiconductors on metal nanostructures is interesting from both fundamental and applied perspectives. The realization of nanostructures with excellent interfaces and material properties that also have controlled optical resonances can be very challenging. Here we report the synthesis and characterization of metal–semiconductor core–shell nanowires. We demonstrate a solution-phase route to obtain stable core–shell metal–Cu₂O nanowires with outstanding control over the resulting structure, in which the noble metal nanowire is used as the nucleation site for epitaxial growth of quasi-monocrystalline Cu₂O shells at room temperature in aqueous solution. We use X-ray and electron diffraction, high-resolution transmission electron microscopy, energy dispersive X-ray spectroscopy, photoluminescence spectroscopy, and absorption spectroscopy, as well as density functional theory calculations, to characterize the core–shell nanowires and verify their structure. Metal–semiconductor core–shell nanowires offer several potential advantages over thin film and traditional nanowire architectures as building blocks for photovoltaics, including efficient carrier collection in radial nanowire junctions and strong optical resonances that can be tuned to maximize absorption.



KEYWORDS: Core–shell nanowire, epitaxial growth, solution phase synthesis, metal–semiconductor heterostructures, quasi-monocrystalline cuprous oxide (Cu₂O), single nanowire quantitative optical absorption measurements

The development of inexpensive and efficient solar cells has been a major research focus over the past 10 years to face the projected increase in global energy consumption.¹ Ideally, the ultimate solar cell would convert light into electricity in the smallest possible volume of material. This desire to minimize volume is not only motivated by the reduced costs associated with using less semiconductor material but also fundamentally linked to a higher solar conversion efficiency. This higher theoretical efficiency has been well documented and arises from two considerations: (1) using less material reduces bulk recombination and thus can boost the open-circuit voltage (V_{oc}),² and (2) reaching full absorption in less material could lead to higher photogenerated carrier densities and thus higher V_{oc} .^{3,4} The light concentration effect has been historically applied using macroscale concentrating optics, and the efficiency enhancement comes via a <60 mV increase of V_{oc} per decade of concentration. For example, this V_{oc} enhancement is largely responsible for the increase in efficiency from 31.3% at 1 sun to 40.7% at 240 sun⁵ in triple-junction solar cells. More recently, researchers have shown that single semiconducting nanowires and nanowire arrays can act as antennas, providing a similar concentration effect without

external optics and employing a reduced amount of material.^{6,7} Furthermore, the possibility to combine materials with high lattice mismatch in heteroepitaxial junctions,^{8–10} and the opportunity to decrease the material volume without compromising light absorption,^{11–13} make the development of nanowire-based solar cells intriguing.^{14–16}

These results motivated us to investigate a novel core–shell nanowire geometry consisting of a metal nanowire coated by an ultrathin semiconductor shell, which theoretically shows superior absorption compared to solid semiconductor nanowires (Figure 1).¹⁷ In this hybrid core–shell geometry there are several resonances with high field intensity in the shell, leading to efficient light absorption in the semiconductor. Furthermore, this geometry is particularly appealing because the metal core can also function as an electrode embedded within the semiconductor that locally collects photogenerated charge carriers;^{18,19} this indeed simplifies the realization of a working device and might reduce fabrication costs. For this scheme to

Received: July 23, 2014

Revised: September 3, 2014

Published: September 18, 2014

work, the quality of the semiconductor and the nature of the interface are extremely important to provide sufficient carrier mobility and to reduce recombination.^{9,14,20} Fabrication of related metal–semiconductor heterostructures has recently attracted a lot of attention,^{21,22} and the synthesis of core–shell nanoparticles with monocrystalline shells has allowed for the exploration of new avenues in fundamental nanomaterial research^{23–25} as well as the demonstration of new technological applications;^{26,27} however, solution-phase synthesis of this class of heterostructures has so far been limited mainly to nanoparticles.^{24,28–31}

Here we report the synthesis and characterization of metal–Cu₂O core–shell nanowires. Cu₂O was chosen as a first model system to demonstrate this concept because it is an earth abundant material with a high absorption coefficient and a band gap close to ideal for the top layer in a tandem solar cell with silicon.³² Additionally, it provides a relatively low lattice mismatch with both Ag and Au (~4%), which have been used for high-performance nanowire transparent electrodes.^{18,19}

We begin by describing the synthetic procedure and resulting morphology and then use numerical simulations and analytical calculations to demonstrate the high electric field intensities in the thin semiconducting shell and the large absorption efficiency that can be reached with these structures. We confirm these theoretical predictions with quantitative single-nanowire absorption measurements. The good agreement with theory gives us confidence to calculate absorption in periodic arrays of these nanowires to predict how they would perform in a macroscopic solar cell. The results show that in our core–shell configuration a 40 nm Cu₂O shell can absorb approximately the same amount of light as a semi-infinite Cu₂O slab without an antireflection coating. Photoluminescence measurements on single nanowires also confirm that carriers are not completely quenched by the local metal contact, and the band gap value is similar to what is observed in bulk films. In addition to the optical properties we provide electron microscopy and X-ray spectroscopy to show that the cuprous oxide shell is spatially uniform, quasi-monocrystalline, pure-phase Cu₂O. Selected area electron diffraction (SAED) and high-resolution transmission electron microscopy (HR-TEM) confirm the epitaxial relationship between the core and the shell. Density functional theory (DFT) calculations provide further insight into the binding configuration at the interface. Finally, the cuprous oxide shell shows no evidence of further oxidation to cupric oxide (CuO) even after extended storage in air. Combined, these results suggest that our core–shell nanowires could be an excellent platform for fundamental studies of metal–semiconductor interfaces, which are critical in many optoelectronic devices. Furthermore, the efficient absorption and local contacting features of such a geometry could have an impact in applications beyond photovoltaics such as sunlight-to-fuel conversion, photodetectors, and light-emitting diodes.

The synthesis of metal–Cu₂O core–shell nanowires (Figure 2) is performed entirely in solution and involves two steps (see Supporting Information for further details): (i) synthesis of metal nanowires via the polyol process in ethylene glycol; (ii) employing metal nanowires as the nucleation site for the growth of a Cu₂O shell at room temperature in water.

Core–shell nanowires with a silver core were chosen to illustrate the structural, chemical, and optical properties of such heterostructures (see Supporting Information for core–shell nanowires with a gold core). The advantage of using Ag versus

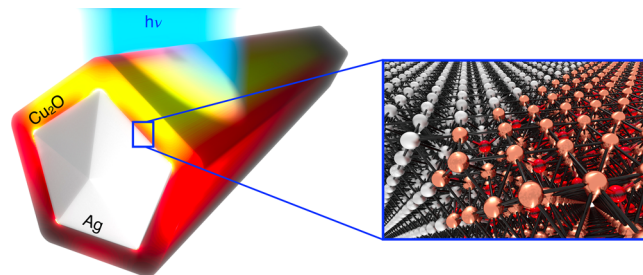


Figure 1. Ag–Cu₂O core–shell nanowires. Artist's impression of a core–shell nanowire illuminated from the top. The light absorption profile is overlaid on the schematic image, and the inset shows the lattice matching at the interface.

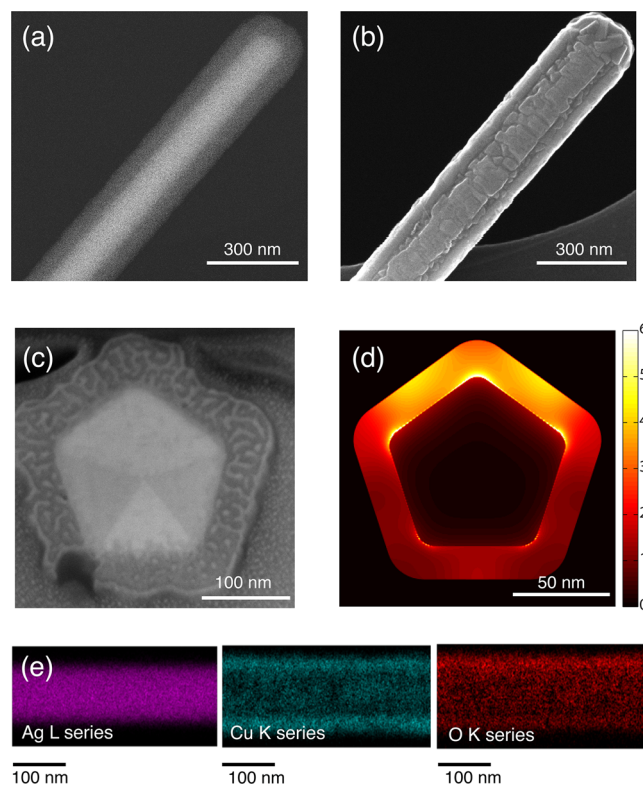


Figure 2. Ag–Cu₂O core–shell nanowire: (a) in-column-detector (ICD) and (b) secondary electrons (SE) image of a Ag–Cu₂O nanowire lying on a substrate; (c) focused ion beam (FIB) cross-sectional view; (d) distribution profile of the total absorbed power averaged over AM 1.5 (unpolarized), calculated from FDTD simulations for a Ag–Cu₂O core–shell nanowire in vacuum. The color scale is in 10⁴ W/m² for a 1 V/m plane wave incident from the top. (e) EDS elemental maps of a Ag–Cu₂O nanowire, for Ag, Cu, and O showing the presence of a core–shell geometry.

Au is the lower cost and the better conductivity. Compared to other metals, such as Cu, Ag is more stable to chemical reactions, but other metals such as Al could be interesting from the optical and economical point of view.

Figure 2c shows a representative cross section of a Ag–Cu₂O nanowire after focused ion beam milling. In the cross-sectional image there is clear contrast between the Ag core and the Cu₂O shell. Interestingly, it is also possible to resolve the five twin planes of the Ag nanowire and appreciate a different contrast for different single-crystalline subunits. Note that Ag nanowires grow from 5-fold twinned decahedral seeds along the [110] direction³³ and therefore feature a pentagonal cross section.

The bright features visible on the shell are due to adsorption of sputtered material during preparation of the cross section. Elemental maps recorded using energy dispersive spectroscopy (EDS) in an SEM verify the elemental distribution in our core–shell nanowires (Figure 2e). The emission intensity of characteristic X-rays is plotted as a function of the electron beam position, for three different X-ray energies, characteristic of Ag (L shell), Cu (K shell), and O (K shell). The three plots in Figure 2e confirm the localization of Ag only in the core of the nanowire and show that X-rays from Cu and O are emitted from a larger region in the radial direction. Note that the intensity in the Cu and O chemical maps is higher at the edge, where the projected shell thickness is higher as expected for the proposed Ag–Cu₂O core–shell nanowire structure. It should be emphasized that different core diameters and shell thicknesses can be achieved by adjusting the synthetic conditions and that other metal nanowires can be employed for the nucleation of the Cu₂O shell with the same synthetic procedure (see Supporting Information Figure S1 for an example of a Au–Cu₂O nanowire).

Within the same synthetic batch, some difference in shell thicknesses can be observed for nanowires with very different core sizes. As the shell growth is typically very fast (1–2 min for first nucleation and growth stage), adjacent nanowires in solution compete for Cu precursor. This means that nanowires with larger cores, which require a larger volume of Cu₂O for the same shell thickness, end up with thinner shells. This often results in higher surface roughness or, in extreme cases, even incomplete shell coverage (see Supporting Information Figure S3).

We used finite-difference time domain (FDTD) to model light absorption in pentagonal Ag–Cu₂O nanowires. The wavelength-dependent absorbed power density in the nanowire was weighted over the AM1.5 solar spectrum and integrated for photon energies above the band gap (290–650 nm). Figure 2d shows a 2D spatial map of the integrated absorbed power. The power profile is averaged over TE and TM polarizations for the best comparison to unpolarized sunlight. From Figure 2d it is clear that most of the absorption occurs in the Cu₂O shell, but there is some parasitic absorption in the metal core (<16%). In order to provide a comparison to a thin-film geometry, in Supporting Information Figure S2 we show the absorbed power distribution for three control systems: a 100 nm thick Ag film (Figure S2a), a 40 nm thick Cu₂O membrane (Figure S2b), and the combination of the previous two (Figure S2c) upon illumination by a plane wave. Note that as for the Ag–Cu₂O nanowire the absorbed power is weighted over the AM1.5 spectrum and integrated from 290 to 650 nm. The maximum of the absorbed power density in the core–shell geometry is 3 times larger than that absorbed in a Cu₂O membrane supported on a Ag film. This corroborates the large optical cross section of this new core–shell nanowire architecture. Note that the dimensions of the Ag–Cu₂O nanowire shown in Figure 2d correspond to the optimum dimensions for the largest absorbed power density (core radius: $r_c = 50$ nm; shell thickness: $t_s = 20$ nm).

To verify the absorption properties of such core–shell nanowires experimentally, we measured the quantitative absorption in both polarizations (Figure 3a). In the TE polarization (electric field polarized perpendicular to the nanowire's axis) the core–shell nanowire shows two resonant absorption peaks in the experimental spectrum, while in TM (electric field polarized along nanowire's axis) only one is

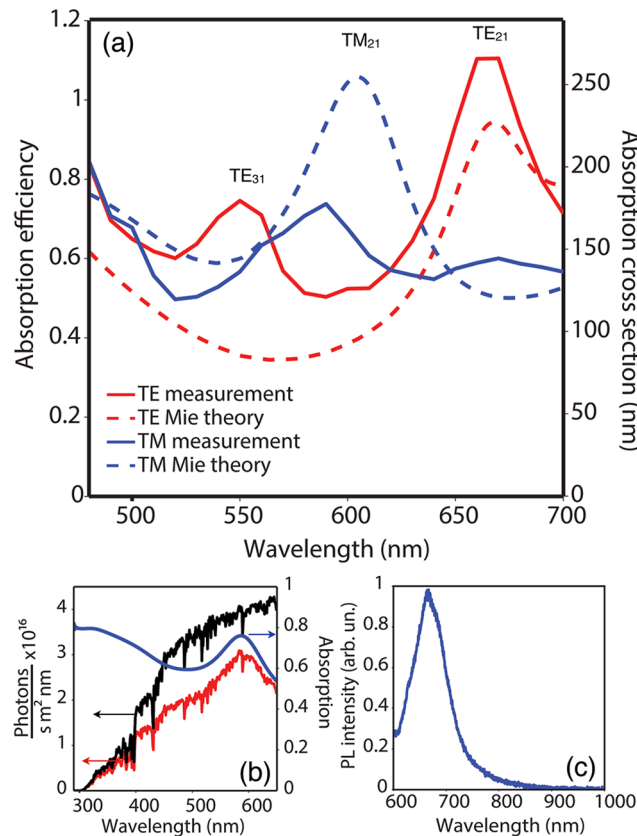


Figure 3. Optical characterization of a single Ag–Cu₂O core–shell nanowire with a core radius of 55 nm and a shell thickness of 65 nm. (a) Experimental (solid lines) and calculated (dashed lines) quantitative absorption spectrum of a single core–shell nanowire in TE (red) and TM (blue) polarizations. (b) FDTD simulation of the photons absorbed in the shell of a Ag–Cu₂O nanowire array weighted over the AM 1.5 (red line); photon flux in the solar spectrum (black line); absorption in the Cu₂O shell before weighting for AM 1.5 (blue line). (c) Photoluminescence emission of a single core–shell nanowire.

visible. Figure 3a compares the measured absorption cross section to Mie theory calculations for a cylindrical core–shell nanowire with roughly the same dimensions (see Supporting Information). There is good agreement between theory and experiment. Since we have verified these quantitative absorption measurements in a simpler silicon nanowire system (which will be discussed in a future publication), we attribute the differences between measurement and theory (in particular, the emergence of a second resonance in TE) to significant surface roughness (see Figure S4 for SEM images). In the smooth cylindrical geometry TE₃₁ is strongly overdamped, but the surface roughness increases the radiative loss rate, which alters the absorption cross section and thus leads to the apparent emergence of resonances.¹⁷ Note that the ratio between the beam diameter, measured by the knife-edge technique, and the core–shell nanowire diameter was taken into account to quantitatively calculate the absorption efficiency reported in Figure 3a.

Interestingly, the absolute values of absorption do not differ substantially from the values calculated for a cylindrical core–shell nanowire, and the measured spectral dependence is similar to calculations for both TE and TM polarizations.

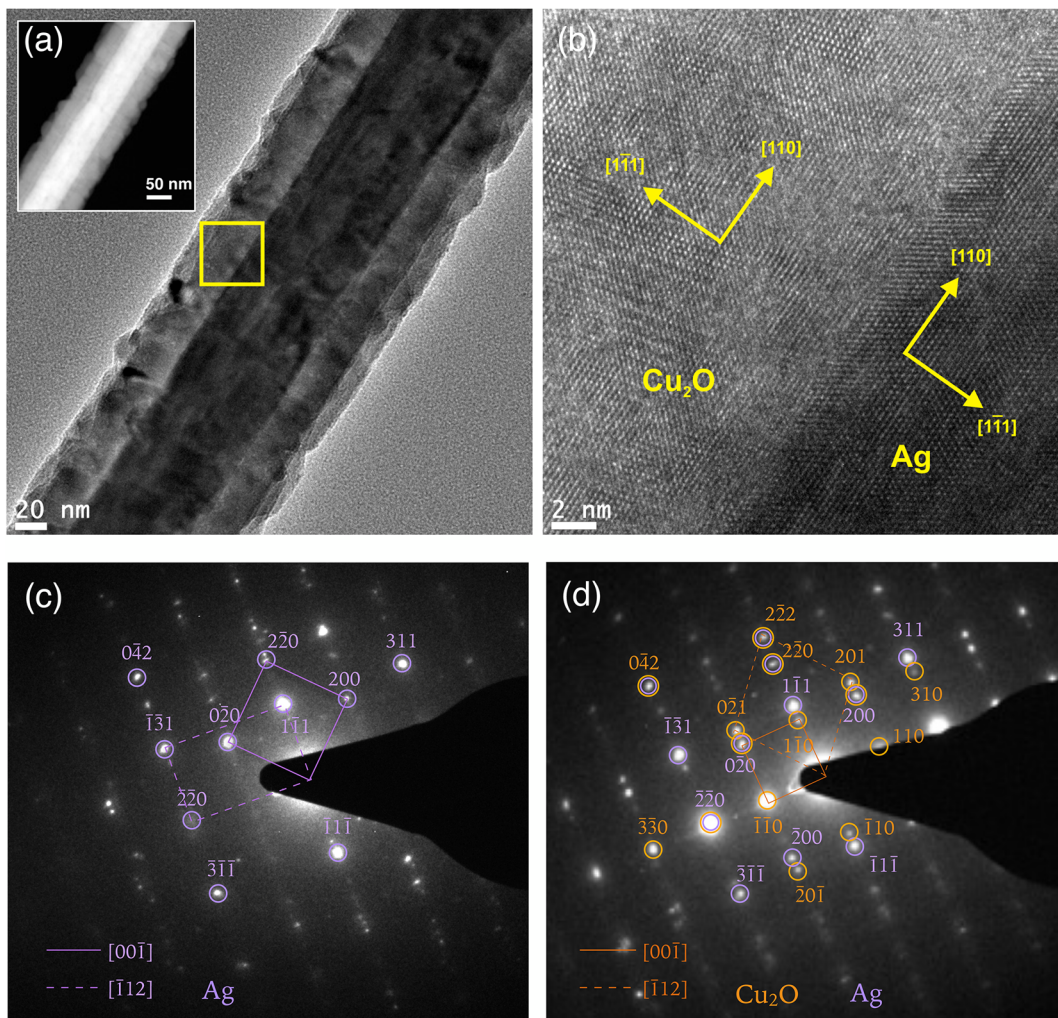


Figure 4. Structural characterization of Ag–Cu₂O core–shell nanowire. (a) Bright field TEM of a representative Ag–Cu₂O core–shell nanowire, showing a neat contrast between Ag core and Cu₂O shell; inset: the HAADF image emphasizes Z contrast in the Ag–Cu₂O nanowire. (b) HRTEM image of the interface between core and shell in the region highlighted in (a). The two lattices match at the interface along the [110] direction and show epitaxial growth. (c, d) SAED pattern for an individual Ag nanowire and Ag–Cu₂O nanowire, respectively. The indexing of the SAED pattern has been performed along [001] and [T12] zone axes and shows a cube-on-cube orientation relationship of the Cu₂O shell on the Ag core. The spot size included the entire core–shell nanowire shown in (a).

To provide a comparison of the absorption properties of Ag–Cu₂O nanowires with bulk absorbing materials, we carried out FDTD simulations of Ag–Cu₂O periodic arrays lying on a perfect electric conductor, with the dimensions used in Mie theory to calculate the absorption spectrum of Figure 3a ($r_c = 55$ nm, $t_s = 65$ nm). The spectral dependence of the absorbed photon flux in the shell material (weighted for the AM1.5 spectrum) in a Ag–Cu₂O nanowire array is presented in Figure 3b (red line), along with the total photon flux in the AM1.5 spectrum (black line) and the absolute absorption (not weighted) fraction in the Cu₂O shell (blue line). The total absorbed flux integrated in the range of 290–650 nm is 66% (absorbed in the Cu₂O shell). With further optimization of the core radius and shell thickness it is possible to achieve a total integrated absorption as large as 72% in the shell material for such a Ag–Cu₂O nanowire array ($r_c = 100$ nm, $t_s = 40$ nm, nanowires touching). For comparison, a semi-infinite Cu₂O film without an antireflection coating absorbs roughly 75% of the AM1.5 spectrum. In the case of a Cu₂O thin film on a perfect electric conductor, an absorption as large as 71% of the AM1.5 spectrum could be achieved for the optimized case (50

nm Cu₂O film thickness). In such a geometry, however, there are no electrical contacts, while in the core–shell geometry, both contacts are already present, and thus shading is taken into account.

In addition to optical absorption measurements, photoluminescence (PL) experiments were performed on individual Ag–Cu₂O nanowires by exciting at a wavelength of 532 nm with a laser (Figure 3c). The band gap luminescence at 670 nm from individual nanowires suggests that the metal–semiconductor interface does not fully quench radiative processes. The emission wavelength is slightly different from what has been observed in bulk Cu₂O which could be related to the lattice mismatch or optical resonances in the nanostructure.^{34–37}

Below we use electron microscopy and X-ray spectroscopy to investigate the quality of the metal–semiconductor interface and to analyze the characteristics of the Cu₂O shell. Figure 4a shows a representative bright field transmission electron microscopy (BF-TEM) image of a Ag–Cu₂O nanowire. The Ag core is clearly visible in the center. The apparent double layer contrast in the Cu₂O shell is the result of a 2D projection

of the 3D pentagonal morphology, whereby Cu_2O shell domains from different pentagonal facets can be overlapping, depending on the orientation of the nanowire on the substrate. The scanning transmission electron microscopy high-angle annular dark-field (STEM-HAADF) image (inset of Figure 4a) displays so-called Z-contrast and highlights the substantial difference in atomic number between the Ag core and the Cu_2O shell. Figure 4b shows a HR-TEM image of the area indicated in Figure 4a. The yellow axes represent the crystallographic directions of core and shell.

Ag and Cu_2O both have a cubic crystal lattice, and Ag has space group $Fm\bar{3}m$ with a lattice parameter of 4.090 \AA ,³⁸ while Cu_2O has space group $Pn\bar{3}m$ with a lattice parameter of 4.269 \AA .³⁹ Interestingly, in the core–shell nanowire, the primary axes of both crystals are mutually aligned, resulting in a cube-on-cube orientation relationship, with a lattice mismatch of 4.4% (see inset in Figure 5a). The crystals are both oriented with

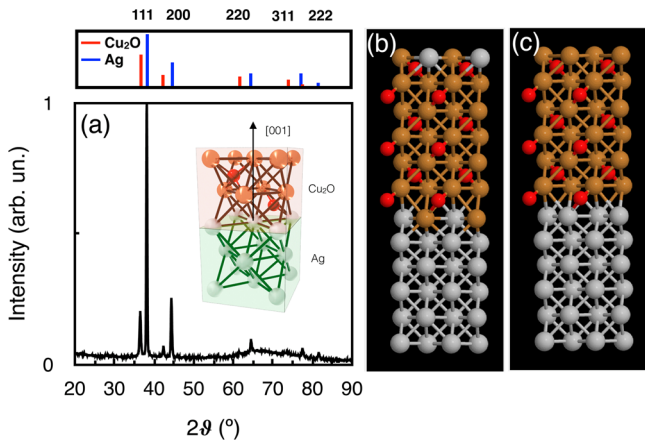


Figure 5. Structural characterization of Ag– Cu_2O core–shell nanowire. (a) XRD of Ag– Cu_2O nanowire ensemble in the range 20° – 90° , showing diffraction peaks of Ag and Cu_2O . Top: reference values for Ag (blue) and Cu_2O (red) diffraction peaks.²³ Inset: artistic impression of the cube-on-cube orientation between the core and the shell material. (b, c) Structural atomic models of the Ag– Cu_2O interface obtained after structural relaxation using DFT calculations for mixed and unmixed Ag/Cu atomic layers, respectively. Brown spheres represent copper atoms, red spheres oxygen atoms, and gray spheres silver atoms.

their [110] axes along the length of the nanowire and have the [111] and [001] axes pointing in lateral directions. From this analysis it is evident that the Cu_2O shell grows epitaxially on the Ag nanowire core, and therefore polyvinylpyrrolidone (PVP), which is known to passivate Ag nanowire facets,³³ must be displaced during the nucleation and growth of Cu_2O , as no interlayer is observed. HR-TEM measurements were performed on multiple Ag– Cu_2O nanowires along various zone axes to confirm the epitaxial growth and showed similar orientations between the Ag core and the Cu_2O shell. In addition, epitaxial growth was observed for core–shell nanowires with larger core diameters (above 200 nm, Figure S3).

The long-range order of the Cu_2O shell, its crystallographic structure and relationship to the underlying Ag lattice were studied by selected area electron diffraction (SAED), by collecting signal from the entire core–shell nanowire shown in Figure 4a. As a reference, a SAED pattern for an individual Ag nanowire is shown in Figure 4c. The diffraction pattern cannot be assigned to a simple FCC crystal because of the

presence of five twinned subcrystals, leading to two individual diffraction patterns superimposed: one along the [001] zone axis (solid line) and one along the [112] zone axis (dashed line).³³

A series of new spots appear in the diffraction pattern of the Ag– Cu_2O core–shell nanowire (Figure 4d), as denoted by the orange circles. Some key features emerge from this pattern: (i) individual spots are observed, as opposed to a continuous ring, demonstrating that the Cu_2O shell on every Ag facet is quasi-monocrystalline; (ii) two sets of superimposed quasi-single-crystal diffraction patterns are observed for Cu_2O , one with square symmetry along the [001] zone axis and one with rhomboidal symmetry along the [112] zone axis, confirming the cube-on-cube crystallographic alignment of the Cu_2O shell with the underlying Ag nanowire crystal, as depicted in the inset of Figure 5a; (iii) epitaxial relationship $(0\bar{2}0)_{\text{Ag}} \parallel (0\bar{2}0)_{\text{Cu}_2\text{O}}$, $(200)_{\text{Ag}} \parallel (200)_{\text{Cu}_2\text{O}}$ and $[00\bar{1}]_{\text{Ag}} \parallel [00\bar{1}]_{\text{Cu}_2\text{O}}$; (iv) epitaxial relationship $(\bar{2}\bar{2}0)_{\text{Ag}} \parallel (\bar{2}\bar{2}0)_{\text{Cu}_2\text{O}}$, $(1\bar{1}1)_{\text{Ag}} \parallel (2\bar{2}2)_{\text{Cu}_2\text{O}}$, and $[\bar{1}12]_{\text{Ag}} \parallel [\bar{1}12]_{\text{Cu}_2\text{O}}$; (v) the presence of two zone axes aligned with those of the Ag core (diffraction spots from the Cu_2O in positions contiguous to those of Ag nanowire pattern) suggests that the crystal orientation for Cu_2O is the same everywhere for a specific Ag nanowire subcrystal, therefore confirming the quasi-monocrystallinity of the shell; (vi) it is interesting to note that the (110) diffraction is forbidden for a Ag nanowire by the FCC structure factor rule (see Figure 4c); however, in the core–shell nanowire a (110) spot is present because of diffraction in Cu_2O , which belongs to the $Pn\bar{3}m$ group. Note that the high intensity of spot $(\bar{2}\bar{2}0)$ is due to the overlap of diffraction along this direction for both core and shell. Also note that diffraction along [110] for Cu_2O occurs along both zone axes and therefore is more intense.

Figure 4d demonstrates that the matching between Ag and Cu_2O lattices occurs for every twinned subcrystal along the whole interface, and it is consistent with HRTEM measurements. The SAED pattern of Figure 4d included signal from the entire core–shell nanowire shown in Figure 4a and is therefore representative of the crystallinity of the Cu_2O shell on a large scale. On the individual nanowire analyzed in Figure 4, there are no signs of either Cu or CuO phases present in the shell material.

The growth process of the Cu_2O shell occurs in three steps:^{23,25} (1) epitaxial nucleation of Cu_2O nanoparticles on the metal substrate, (2) Cu_2O nanoparticle growth until the reagents are consumed, and (3) crystal reconstruction to release stress created during the growth. The shell consists of multiple grains that are aligned in rows along each of the five Ag{100} facets, as borne out by SAED measurements on the entire core–shell nanowire. These grains might crystallographically be slightly misaligned and not have exactly the same height because of local differences in the growth rate, resulting in surface roughness, which causes the contrast visible in the SEM images (Figure 2b and Figures S3 and S4). However, they all follow the same orientation relationship with the five subcrystals in the pentagonal Ag core, and therefore their mutual crystallographic misalignment is less than what is detectable in SAED. The morphological and structural configuration of the Cu_2O shell is a result of the growth process, whereby Cu_2O nucleates simultaneously at many points along the Ag nanowire. These Cu_2O nuclei grow until their edges touch, leading to rows of almost perfectly aligned Cu_2O grains along each of the pentagonal Ag facets. The five

elongated Cu₂O domains covering the Ag nanowire are therefore nearly single crystalline but may contain planar defects such as low-angle tilt boundaries and low-angle twist boundaries or dislocations. From this point of view, it is more appropriate to call it a *quasi-monocrystal*, using a terminology employed in similar materials for silicon photovoltaics.⁴⁰ These low-angle planar defects are indeed not visible in the SAED pattern, showing that the angle misalignment between the grains has to be very low not to be resolved. Although these low-angle planar defects are not visible in the SAED pattern, in bright-field TEM images it is sometimes possible to observe the existence of both low-angle grain boundary regions as well as fully monocrystalline regions (Figure S5).

In order to demonstrate that the growth of pure Cu₂O is achievable in large ensembles, we performed XRD analysis on a thick film of Ag–Cu₂O nanowires drop-cast from solution in a 2θ range of 20°–90° (see Figure 5a). Intense diffraction peaks matching crystalline Ag were observed, along with peaks matching Cu₂O, as labeled in the spectrum of Figure 5a. For comparison, reference values for both Ag (blue) and Cu₂O (red) are reported on the top of the figure. The low intensity of the Cu₂O reflection peak is most likely due to the low Cu₂O ratio in the core–shell nanowire sample employed for the measurements. Importantly, no undesirable phases such as copper(II) oxide (CuO), Cu, mixed metal oxides, or intermetallics were detected even after storage for 6 months in air, revealing the stability of the heterostructure interface and uniformity on a large scale.

While the HR-TEM, SAED, and XRD results confirm epitaxial growth of Cu₂O from the Ag surface, they do not provide information about the atomic binding configurations at the Ag–Cu₂O interface. Therefore, plane-wave DFT calculations^{41,42} using the generalized gradient approximation (GGA) were performed. A plausible atomic model was constructed in which the FCC metal (sub)lattice of Ag/Cu atoms is continuous across the Ag{001}/Cu₂O{001} interface. Two models were considered: one in which the interface contains Ag/Cu mixed atomic layers (Figure 5b) and one model without mixed layers (Figure 5c). The difference in interfacial energy between the two models is very small, indicating that both types of interfaces may be formed. More details are given in the Supporting Information. Free energy calculations and Auger spectroscopy results reported on another noble metal–Cu₂O interface, namely Au–Cu₂O,⁴³ are consistent with the DFT result of Figure 5b, which shows that there is no Ag–O bonding at the interface.

We have shown that under the appropriate experimental conditions silver nanowires can be used as a nucleation site for the epitaxial growth of quasi-monocrystalline, pure phase cuprous oxide shells at room temperature in a water environment. SAED, HRTEM, and XRD analyses prove that the shell consists of pure Cu₂O, which is unusual in bulk Cu₂O samples, whose oxidation to CuO has been reported to occur in ambient conditions.⁴⁴ By tuning the synthetic parameters, various core diameters and shell thicknesses can be obtained, leading to fine control over optical resonances and ultimately light absorption. We showed that the optical response of Ag–Cu₂O is in good agreement with theory/simulations, and most of the power absorption takes place in the semiconductor shell due to the nature of the resonances. FDTD simulations show a 3-fold increase of the maximum absorbed power density within the semiconductor shell, compared to a thin Cu₂O membrane with the same dimensions supported on a Ag film.

Other oxides with similar band gaps and lattice constants, such as CoO, can potentially be interesting within this application as well. Metal sulfides such as Cu₂S or CdS could also be intriguing absorbing layers, but they require a core material that does not react with sulfur (such as Au). Indeed, heterostructures with a Au core and a CdS shell have been synthesized by a nonepitaxial method using an amorphous intermediate,²¹ and this approach might be extendable to nanowire core–shell systems with large lattice mismatches.

By combining high quality quasi-monocrystalline materials made at room temperature and efficient light absorption in extraordinarily thin absorbing layers, we expect substantial improvements in the performance of solar devices based on Ag–Cu₂O core–shell nanowires. On the other hand, the lower material consumption and the employment of a simple and inexpensive fabrication process—the solution-phase synthesis—could have a large impact on reducing the module cost. Finally, the opportunity to achieve high quality quasi-monocrystalline semiconductor grown on a metal contact with an excellent interface is indeed compelling to pursue fundamental studies on semiconductor properties at the nanoscale.

■ ASSOCIATED CONTENT

S Supporting Information

Details on the synthesis of Ag nanowires and the Cu₂O shell growth, experimental details on the structural and optical characterization, details on the density functional theory (DFT) calculations, and additional SEM and TEM images. This material is available free of charge via the Internet at <http://pubs.acs.org>.

■ AUTHOR INFORMATION

Corresponding Author

*E-mail garnett@amolf.nl (E.C.G.).

Notes

The authors declare no competing financial interest.

■ ACKNOWLEDGMENTS

The authors acknowledge AMOLF technical support, Henk-Jan Boluijt for the realization of the schematic drawing in Figure 1a, and Dr. Toon Coenen, Dr. Sarah Britzman, and Sebastian Oener for helpful discussions. We thank Hans Meeldijk (Utrecht Univ.) for TEM assistance. Furthermore, we acknowledge support from the Light Management in New Photovoltaic Materials (LMPV) center at AMOLF. This work is part of the research program of the Foundation for Fundamental Research on Matter (FOM), which is part of The Netherlands Organization for Scientific Research (NWO). The research leading to these results has received funding from the European Research Council under the European Union's Seventh Framework Programme (FP/2007-2013)/ERC Grant Agreement no. 337328, "NanoEnabledPV".

■ REFERENCES

- (1) Lewis, N. S.; Nocera, D. G. Powering the planet: Chemical challenges in solar energy utilization. *Proc. Natl. Acad. Sci. U. S. A.* **2007**, *104* (50), 20142–20142.
- (2) Green, M. A. Limits on the open-circuit voltage and efficiency of silicon solar cells imposed by intrinsic Auger processes. *IEEE Trans.* **1984**, *31* (5), 671–678.

- (3) Cotal, H.; Fetzer, C.; Boisvert, J.; Kinsey, G.; King, R.; Hebert, P.; Yoon, H.; Karam, N. III-V multijunction solar cells for concentrating photovoltaics. *Energy Environ. Sci.* **2009**, *2* (2), 174–192.
- (4) Wurfel, P. *Physics of Solar Cells*; Wiley-VCH: Weinheim, 2009.
- (5) King, R. R.; Law, D. C.; Edmondson, K. M.; Fetzer, C. M.; Kinsey, G. S.; Yoon, H.; Sherif, R. A.; Karam, N. H. 40% efficient metamorphic GaInP/GaInAs/Ge multijunction solar cells. *Appl. Phys. Lett.* **2007**, *90*, (18).
- (6) Brongersma, M. L.; Cui, Y.; Fan, S. H. Light management for photovoltaics using high-index nanostructures. *Nat. Mater.* **2014**, *13* (5), 451–460.
- (7) Cao, L. Y.; White, J. S.; Park, J. S.; Schuller, J. A.; Clemens, B. M.; Brongersma, M. L. Engineering light absorption in semiconductor nanowire devices. *Nat. Mater.* **2009**, *8* (8), 643–647.
- (8) Tang, J. Y.; Huo, Z. Y.; Britzman, S.; Gao, H. W.; Yang, P. D. Solution-processed core-shell nanowires for efficient photovoltaic cells. *Nat. Nanotechnol.* **2011**, *6* (9), 568–572.
- (9) Wu, Y.; Xiang, J.; Yang, C.; Lu, W.; Lieber, C. M. Single-crystal metallic nanowires and metal/semiconductor nanowire heterostructures. *Nature* **2004**, *430* (7000), 704–704.
- (10) Lauhon, L. J.; Gudiksen, M. S.; Wang, C. L.; Lieber, C. M. Epitaxial core-shell and core-multishell nanowire heterostructures. *Nature* **2002**, *420* (6911), 57–61.
- (11) Garnett, E.; Yang, P. D. Light trapping in silicon nanowire solar cells. *Nano Lett.* **2010**, *10* (3), 1082–1087.
- (12) Wallentin, J.; Anttu, N.; Asoli, D.; Huffman, M.; Aberg, I.; Magnusson, M. H.; Siefer, G.; Fuss-Kaiulweit, P.; Dimroth, F.; Witzigmann, B.; Xu, H. Q.; Samuelson, L.; Deppert, K.; Borgstrom, M. T. InP nanowire array solar cells achieving 13.8% efficiency by exceeding the ray optics limit. *Science* **2013**, *339* (6123), 1057–1060.
- (13) Pala, R. A.; Liu, J. S. Q.; Barnard, E. S.; Askarov, D.; Garnett, E. C.; Fan, S. H.; Brongersma, M. L. Optimization of non-periodic plasmonic light-trapping layers for thin-film solar cells. *Nat. Commun.* **2013**, *4*.
- (14) Tian, B.; Kempa, T. J.; Lieber, C. M. Single nanowire photovoltaics. *Chem. Soc. Rev.* **2009**, *38* (1), 16–24.
- (15) Krogstrup, P.; Jorgensen, H. I.; Heiss, M.; Demichel, O.; Holm, J. V.; Aagesen, M.; Nygard, J.; Morral, A. F. I. Single-nanowire solar cells beyond the Shockley-Queisser limit. *Nat. Photonics* **2013**, *7* (4), 306–310.
- (16) Garnett, E. C.; Brongersma, M. L.; Cui, Y.; McGehee, M. D. Nanowire solar cells. *Annu. Rev. Mater. Res.* **2011**, *41*, 269–295.
- (17) Mann, S. A.; Garnett, E. C. Extreme light absorption in thin semiconductor films wrapped around metal nanowires. *Nano Lett.* **2013**, *13* (7), 3173–3178.
- (18) Garnett, E. C.; Cai, W. S.; Cha, J. J.; Mahmood, F.; Connor, S. T.; Christoforo, M. G.; Cui, Y.; McGehee, M. D.; Brongersma, M. L. Self-limited plasmonic welding of silver nanowire junctions. *Nat. Mater.* **2012**, *11* (3), 241–249.
- (19) Wu, H.; Kong, D. S.; Ruan, Z. C.; Hsu, P. C.; Wang, S.; Yu, Z. F.; Carney, T. J.; Hu, L. B.; Fan, S. H.; Cui, Y. A transparent electrode based on a metal nanotrough network. *Nat. Nanotechnol.* **2013**, *8* (6), 421–425.
- (20) Fan, Z. Y.; Razavi, H.; Do, J. W.; Moriwaki, A.; Ergen, O.; Chueh, Y. L.; Leu, P. W.; Ho, J. C.; Takahashi, T.; Reichertz, L. A.; Neale, S.; Yu, K.; Wu, M.; Ager, J. W.; Javey, A. Three-dimensional nanopillar-array photovoltaics on low-cost and flexible substrates. *Nat. Mater.* **2009**, *8* (8), 648–653.
- (21) Lambright, S.; Butaeva, E.; Razgoniaeva, N.; Hopkins, T.; Smith, B.; Perera, D.; Corbin, J.; Khon, E.; Thomas, R.; Moroz, P.; Mereshchenko, A.; Tarnovsky, A.; Zamkov, M. Enhanced lifetime of excitons in nonepitaxial Au/CdS core/shell nanocrystals. *ACS Nano* **2014**, *8* (1), 352–361.
- (22) Ha, E.; Lee, L. Y.; Wang, J.; Li, F.; Wong, K. Y.; Tsang, S. C. Significant enhancement in photocatalytic reduction of water to hydrogen by Au/Cu₂ZnSnS₄ nanostructure. *Adv. Mater.* **2014**, *26* (21), 3496–500.
- (23) Kuo, C. H.; Hua, T. E.; Huang, M. H. Au nanocrystal-directed growth of Au-Cu₂O core-shell heterostructures with precise morphological control. *J. Am. Chem. Soc.* **2009**, *131* (49), 17871–17878.
- (24) Jiang, R.; Li, B.; Fang, C.; Wang, J. Metal/semiconductor hybrid nanostructures for plasmon-enhanced applications. *Adv. Mater.* **2014**, DOI: 10.1002/adma.201400203.
- (25) Meir, N.; Plante, I. J. L.; Flomin, K.; Chockler, E.; Moshofsky, B.; Diab, M.; Volokh, M.; Mokari, T. Studying the chemical, optical and catalytic properties of noble metal (Pt, Pd, Ag, Au)-Cu₂O core-shell nanostructures grown via a general approach. *J. Mater. Chem. A* **2013**, *1* (5), 1763–1769.
- (26) Li, J. T.; Cushing, S. K.; Bright, J.; Meng, F. K.; Senty, T. R.; Zheng, P.; Bristow, A. D.; Wu, N. Q. Ag@Cu₂O core-shell nanoparticles as visible-light plasmonic photocatalysts. *ACS Catal.* **2013**, *3* (1), 47–51.
- (27) Cushing, S. K.; Li, J. T.; Meng, F. K.; Senty, T. R.; Suri, S.; Zhi, M. J.; Li, M.; Bristow, A. D.; Wu, N. Q. Photocatalytic activity enhanced by plasmonic resonant energy transfer from metal to semiconductor. *J. Am. Chem. Soc.* **2012**, *134* (36), 15033–15041.
- (28) Sun, H.; He, J. T.; Wang, J. Y.; Zhang, S. Y.; Liu, C. C.; Sritharan, T.; Mhaisalkar, S.; Han, M. Y.; Wang, D.; Chen, H. Y. Investigating the multiple roles of polyvinylpyrrolidone for a general methodology of oxide encapsulation. *J. Am. Chem. Soc.* **2013**, *135* (24), 9099–9110.
- (29) Zhang, J. T.; Tang, Y.; Weng, L.; Ouyang, M. Versatile strategy for precisely tailored core@shell nanostructures with single shell layer accuracy: The case of metallic shell. *Nano Lett.* **2009**, *9* (12), 4061–4065.
- (30) Jin, M. S.; Zhang, H.; Wang, J. G.; Zhong, X. L.; Lu, N.; Li, Z. Y.; Xie, Z. X.; Kim, M. J.; Xia, Y. N. Copper can still be epitaxially deposited on palladium nanocrystals to generate core-shell nanocubes despite their large lattice mismatch. *ACS Nano* **2012**, *6* (3), 2566–2573.
- (31) Zhang, L.; Jing, H.; Boisvert, G.; He, J. Z.; Wang, H. Geometry control and optical tunability of metal-cuprous oxide core-shell nanoparticles. *ACS Nano* **2012**, *6* (4), 3514–3527.
- (32) Bailey, Z. M.; McGehee, M. D. Modeling low cost hybrid tandem photovoltaics with the potential for efficiencies exceeding 20%. *Energy Environ. Sci.* **2012**, *5* (11), 9173–9179.
- (33) Sun, Y. G.; Mayers, B.; Herricks, T.; Xia, Y. N. Polyol synthesis of uniform silver nanowires: A plausible growth mechanism and the supporting evidence. *Nano Lett.* **2003**, *3* (7), 955–960.
- (34) Jang, J. I. A unique system hosting various excitonic matter and exhibiting large third-order nonlinear optical responses. *Optoelectronics - Materials and Techniques*, 2011; DOI 10.5772/18416.
- (35) Li, J. Q.; Mei, Z. X.; Ye, D. Q.; Liang, H. L.; Liu, L. S.; Liu, Y. P.; Galeckas, A.; Kuznetsov, A. Y.; Du, X. L. Engineering of optically defect free Cu₂O enabling exciton luminescence at room temperature. *Opt. Mater. Express* **2013**, *3* (12), 2072–2077.
- (36) Biccari, F. *Defects and Doping in Cu₂O*; University of Rome: Rome, 2012.
- (37) Gu, Q.; Wang, B. Correlation between structural defects and optical properties of Cu₂O nanowires grown by thermal oxidation. arXiv:1012.5338, 2011.
- (38) Srnova-Sloufova, I.; Lednický, F.; Gemperle, A.; Gemperlova, J. Core-shell (Ag)Au bimetallic nanoparticles: Analysis of transmission electron microscopy images. *Langmuir* **2000**, *16* (25), 9928–9935.
- (39) Oba, F.; Ernst, F.; Yu, Y. S.; Liu, R.; Kothari, M.; Switzer, J. A. Epitaxial growth of cuprous oxide electrodeposited onto semiconductor and metal substrates. *J. Am. Ceram. Soc.* **2005**, *88* (2), 253–270.
- (40) Ervik, T.; Stokkan, G.; Buonassisi, T.; Mjos, O.; Lohne, O. Dislocation formation in seeds for quasi-monocrystalline silicon for solar cells. *Acta Mater.* **2014**, *67*, 199–206.
- (41) Kresse, G.; Hafner, J. Ab initio molecular-dynamics for liquid-metals. *Phys. Rev. B* **1993**, *47* (1), 558–561.
- (42) Kresse, G.; Furthmüller, J. Efficiency of ab-initio total energy calculations for metals and semiconductors using a plane-wave basis set. *Comput. Mater. Sci.* **1996**, *6* (1), 15–50.

(43) Olsen, L. C.; Addis, F. W.; Miller, W. Experimental and theoretical studies of Cu₂O solar cells. *Sol. Cells* **1982–1983**, *7*, 247–279.

(44) Ram, S.; Mitra, C. Formation of stable Cu₂O nanocrystals in a new orthorhombic crystal structure. *Mater. Sci. Eng., A* **2001**, *304*, 805–809.